# Supporting Information

# Polarisation insensitive multifunctional metasurfaces based on all-dielectric nanowaveguides

*Nasir Mahmood,*[†a,b,c] *Inki Kim,*[†d] *Muhammad Qasim Mehmood,*[†a] *Heongyeong Jeong,*[†d] *Ali Akbar,*[e] *Dasol Lee,*[d] *Murtaza Saleem,*[e] *Muhammad Zubair,*[a] *Muhammad Sabieh Anwar,*[*e] *Farooq Ahmad Tahir*[*b] *and Junsuk Rho*[*d,f,g]

[a] Department of Electrical Engineering, Information Technology University of the Punjab, Lahore 54000, Pakistan

[b] Research Institute for Microwave and Millimeter-wave Studies (RIMMS), National University of Sciences and Technology (NUST), Islamabad 46000, Pakistan

[c] Department of Electrical Engineering, The University of Lahore, 1–KM Defense Road, Lahore 54000, Pakistan

[d] Department of Mechanical Engineering, Pohang University of Science and Technology (POSTECH), Pohang 37673, Republic of Korea

[e] Department of Physics, Syed Babar Ali School of Science and Engineering, (SBASSE), Lahore University of Management Sciences (LUMS), Opposite Sector U, D.H.A. Lahore 54792, Pakistan

[f] Department of Chemical Engineering, Pohang University of Science and Technology (POSTECH), Pohang 37673, Republic of Korea

[g] National Institute of Nanomaterials Technology (NINT), Pohang 37673, Republic of Korea

[†]These authors contributed equally to this work.

*Email: sabieh@lums.edu.pk, farooq.tahir@seecs.edu.pk, jsrho@postech.ac.kr

**Maxwell's equations analysis for the dielectric waveguide model**

Maxwell's equations in a source free region can be written as

$$\nabla \times \bar{E} = -j\omega\mu\bar{H} \tag{S1}$$

$$\nabla \times \bar{H} = j\omega\epsilon\bar{E} \tag{S2}$$

The Helmholtz equation and field components can be described as

$$\nabla^2\bar{E} + \omega^2\mu\epsilon\bar{E} = 0 \tag{S3}$$

$$\nabla^2\bar{H} + \omega^2\mu\epsilon\bar{H} = 0 \tag{S4}$$

$$\bar{E}(r,t) = \bar{E}(r,\varphi)e^{j(\omega t-\beta z)} \tag{S5}$$

$$\bar{H}(r,t) = \bar{H}(r,\varphi)e^{j(\omega t-\beta z)} \tag{S6}$$

Using this, Maxwell's equations can now be written in terms of three components in cylindrical coordinates for each field vector $\left(E_r, E_\varphi, E_z \text{ and } H_r, H_\varphi, H_z\right)$. These are presented below

$$j\omega\epsilon E_r = j\beta H_\varphi + \frac{1}{r}\frac{\partial}{\partial\varphi}H_z \tag{S7}$$

$$j\omega\epsilon E_\varphi = -j\beta H_r - \frac{\partial}{\partial r}H_z \tag{S8}$$

$$j\omega\epsilon E_z = -\frac{1}{r}\frac{\partial}{\partial\varphi}H_r + \frac{1}{r}\frac{\partial}{\partial r}(rH_\varphi) \tag{S9}$$

$$-j\omega\mu H_r = j\beta E_\varphi + \frac{1}{r}\frac{\partial}{\partial\varphi}E_z \tag{S10}$$

$$-j\omega\mu H_\varphi = -j\beta E_r - \frac{\partial}{\partial r}E_z \tag{S11}$$

$$-j\omega\mu H_z = -\frac{1}{r}\frac{\partial}{\partial\varphi}E_r + \frac{1}{r}\frac{\partial}{\partial r}(rE_\varphi) \tag{S12}$$

The six equations above (S7–S12) can be solved for the two transverse components ($E_r, E_\varphi$ and $H_r, H_\varphi$)) of each field vector in terms of longitudinal components ($E_z$ and $H_z$) as

$$E_r = \frac{-j}{{k_c}^2}\left(\beta\frac{\partial}{\partial r}E_z + \frac{\omega\mu}{r}\frac{\partial}{\partial\varphi}H_z\right) \tag{S13}$$

$$E_\varphi = \frac{-j}{{k_c}^2}\left(\frac{\beta}{r}\frac{\partial}{\partial\varphi}E_z - \omega\mu\frac{\partial}{\partial r}H_z\right) \tag{S14}$$

$$H_r = \frac{-j}{{k_c}^2}\left(\beta\frac{\partial}{\partial r}H_z - \frac{\omega\mu}{r}\frac{\partial}{\partial\varphi}E_z\right) \tag{S15}$$

$$H_\varphi = \frac{-j}{{k_c}^2}\left(\frac{\beta}{r}\frac{\partial}{\partial\varphi}H_z + \omega\mu\frac{\partial}{\partial r}E_z\right) \tag{S16}$$

Where, $k_c = \sqrt{\omega^2\epsilon\mu - \beta^2}$, is defined as the cut-off wavenumber.

Using these solutions, the longitudinal and transverse components of fields for cylindrical indexed–waveguide are determined. Further mathematical treatment reveals the following field components for the confined modes inside the core ($r < a$).

$$E_r(r,t) = \frac{-i\beta}{p^2}\left(ApJ_l'(pr) + \frac{i\omega\mu l}{\beta r}BJ_l(pr)\right)exp[i(\omega t + l\varphi - \beta z)] \tag{S17}$$

$$E_\varphi(r,t) = \frac{-i\beta}{p^2}\left(\frac{il}{r}AJ_l(pr) - \frac{\omega\mu}{\beta}BpJ_l'(pr)\right)exp[i(\omega t + l\varphi - \beta z)] \tag{S18}$$

$$E_z(r,t) = AJ_l(pr)exp[i(\omega t + l\varphi - \beta z)] \tag{S19}$$

$$H_r(r,t) = \frac{-i\beta}{p^2}\left(BpJ_l'(pr) - \frac{i\omega\varepsilon_1 l}{\beta r}AJ_l(pr)\right)exp[i(\omega t + l\varphi - \beta z)] \tag{S20}$$

$$H_\varphi(r,t) = \frac{-i\beta}{p^2}\left(\frac{il}{r}BJ_l(pr) + \frac{\omega\epsilon_1}{\beta}ApJ_l'(hr)\right)exp[i(\omega t + l\varphi - \beta z)] \tag{S21}$$

$$H_z(r,t) = BJ_l(pr)exp[i(\omega t + l\varphi - \beta z)] \tag{S22}$$

Similarly, the field components of the confined mode inside the cladding ($r > a$) are given by

$$E_r(r,t) = \frac{i\beta}{q^2}\left(CqK_l'(qr) + \frac{i\omega\mu l}{\beta r}DK_l(qr)\right)exp[i(\omega t + l\varphi - \beta z)] \tag{S23}$$

$$E_\varphi(r,t) = \frac{i\beta}{q^2}\left(\frac{il}{r}CK_l(qr) - \frac{\omega\mu}{\beta}DqK_l'(qr)\right)exp[i(\omega t + l\varphi - \beta z)] \tag{S24}$$

$$E_z(r,t) = CK_l(qr)exp[i(\omega t + l\varphi - \beta z)] \tag{S25}$$

$$H_r(r,t) = \frac{i\beta}{q^2}\left(DqK_l'(qr) - \frac{i\omega\varepsilon_2 l}{\beta r}CK_l(qr)\right)\exp[i(\omega t + l\varphi - \beta z)] \tag{S26}$$

$$H_\varphi(r,t) = \frac{i\beta}{q^2}\left(\frac{il}{r}DK_l(qr) + \frac{\omega\epsilon_2}{\beta}CqK_l'(qr)\right)\exp[i(\omega t + l\varphi - \beta z)] \tag{S27}$$

$$H_z(r,t) = DK_l(qr)exp[i(\omega t + l\varphi - \beta z)] \tag{S28}$$

where $A$, $B$, $C$ and $D$ are arbitrary constants that are determined from the boundary conditions. The relation of parameters $p$ and $q$ with the propagation constant is defined as $p = \left[\left(\frac{n_c\omega}{c}\right)^2 - \beta^2\right]^{1/2}$ and $q = \left[\beta^2 - \left(\frac{n_a\omega}{c}\right)^2\right]^{1/2}$ and $J_l'(pr) = dJ_l(pr)/d(pr)$ , $K_l'(qr) = dK_l(qr)/d(qr)$ , $\epsilon_1 = \epsilon_0 n_c^2$ and $\epsilon_2 = \epsilon_0 n_a^2$ , where $J$ and $K$ represent Bessel and modified Bessel Functions respectively.

For the existence of confined modes, longitudinal components in the core (Eqn S19 and S22) and cladding (Eqn S24 and S27) require $p^2 > 0$ and $q^2 > 0$, which translates to the condition $n_c k_0 > \beta > n_a k_0$. This relation indicates that the ratio of propagation constants of the material and air must remain within the limits of $n_c$ and $n_a$ . At radius $r = a$ , the previously mentioned electromagnetic field components must satisfy the boundary conditions of $E_\varphi, E_z, H_\varphi$ and $H_z$ being continuous at the interface. These conditions yield the following additional constraints:

$$AJ_l(pa) - CK_l(qa) = 0 \qquad (S29)$$

$$A\left(\frac{il}{p^2 a}J_l(pa)\right) + B\left(-\frac{\omega\mu}{p\beta}J_l'(pa)\right) + C\left(\frac{il}{q^2 a}K_l(qa)\right) + D\left(-\frac{\omega\mu}{q\beta}K_l'(qa)\right) = 0 \qquad (S30)$$

$$BJ_l(pa) - DK_l(qa) = 0 \qquad (S31)$$

$$A\left(\frac{\omega\varepsilon_1}{p\beta}J_l'(pa)\right) + B\left(\frac{il}{p^2 a}J_l(pa)\right) + C\left(\frac{\omega\varepsilon_2}{q\beta}K_l'(qa)\right) + D\left(\frac{il}{q^2 a}K_l(qa)\right) = 0 \qquad (S32)$$

## Boundary conditions of the simulation

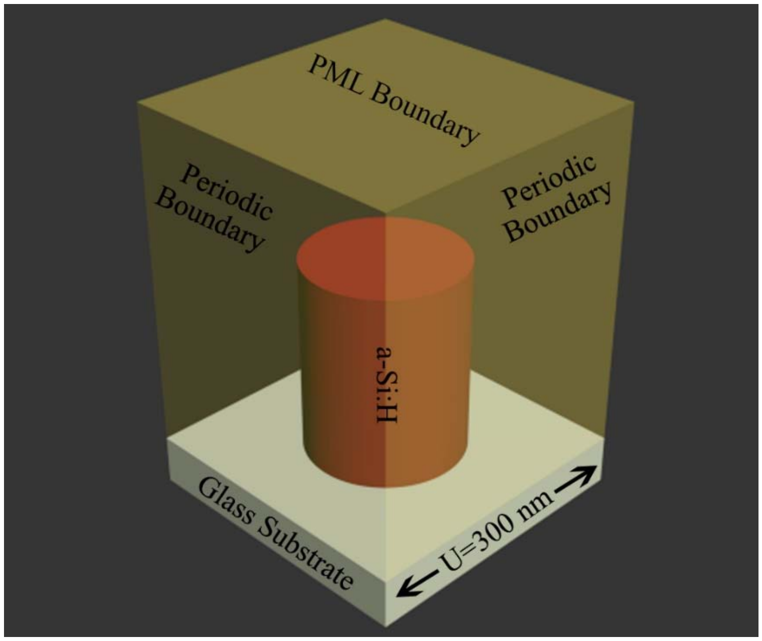


**Fig. S1.** Schematic drawing of numerically simulated unit cell. Nanowaveguide of hydrogenated amorphous silicon (a–Si:H) in cylindrical shaped is deposited on the glass substrate. A full wave Finite Difference Time Domain (FDTD) Solution software from Lumerical Inc. is used to perform the simulations of the unit cell with periodic boundary conditions are used in *x*–*y* direction while perfect matching boundaries are used in propagation direction (*z*). Above mentioned configuration is used to optimise the parameters (range of diameter and period) of the building block.

**Extinction coefficient of a-Si:H**

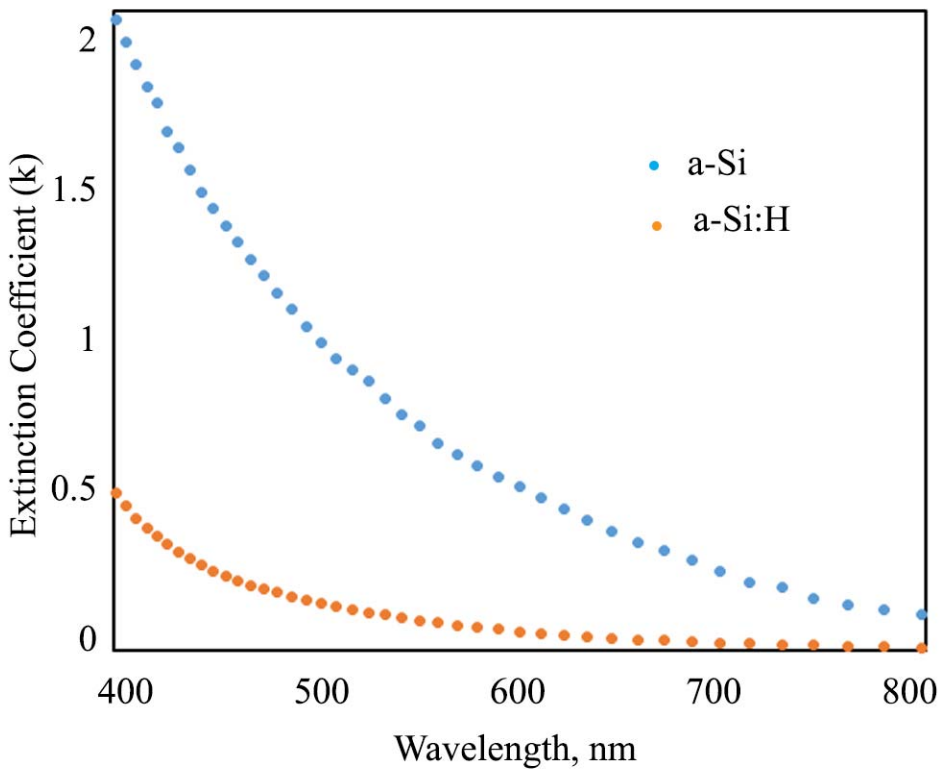


**Fig. S2.** Comparison of extinction coefficient of a–Si:H and a–Si.

**Dielectric indexed waveguide model**

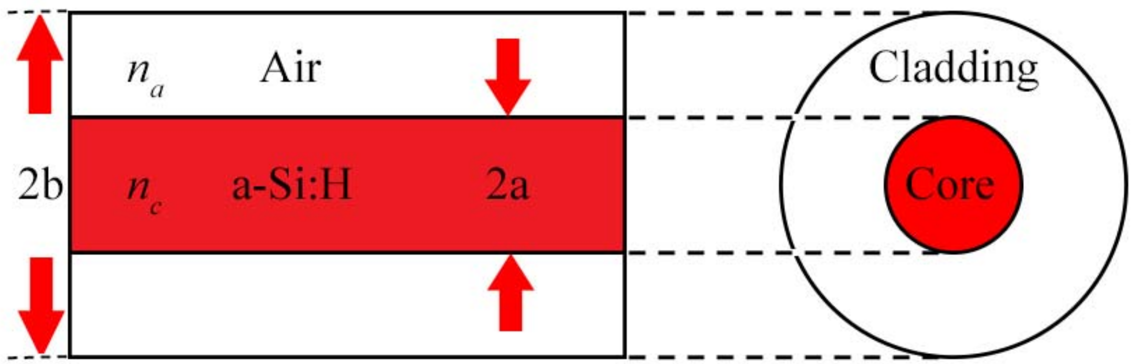


**Fig. S3.** Schematic of symmetric circular dielectric indexed waveguide, represent the radius of core with a and clad with b. Refractive index of dielectric core is represented as $n_c$ and cladding with $n_a$. Here, 400 nm thick a–Si:H is used as the core material and air represents the cladding section.

**Effective refractive index in the waveguide**

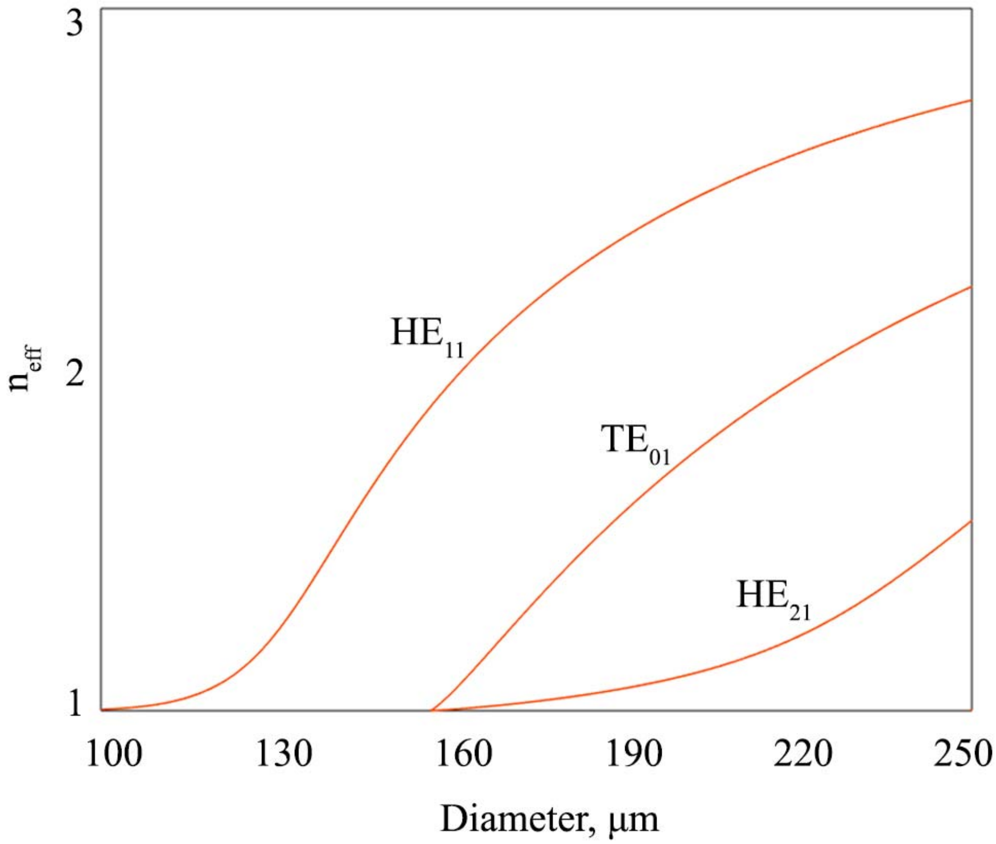


**Fig. S4.** Normalised propagation constant or effective refractive index as a function of diameter for some low order modes of an indexed-waveguide. $HE_{11}$ mode is characterised as fundamental mode with no cutoff frequency thus can propagate for any frequency. It is apparent that at cutoff, each propagating mode has effective refractive index equal to $n_a$, revealing that fields penetrate well into the clad, resulting in poor mode confinement into the core ]hydrogenated amorphous silicon (a–Si:H)_. Away from the cutoff, the effective refractive index approaches $n_c$, representing the tight confinement of propagating mode in the core.

**Device efficiency calculation**

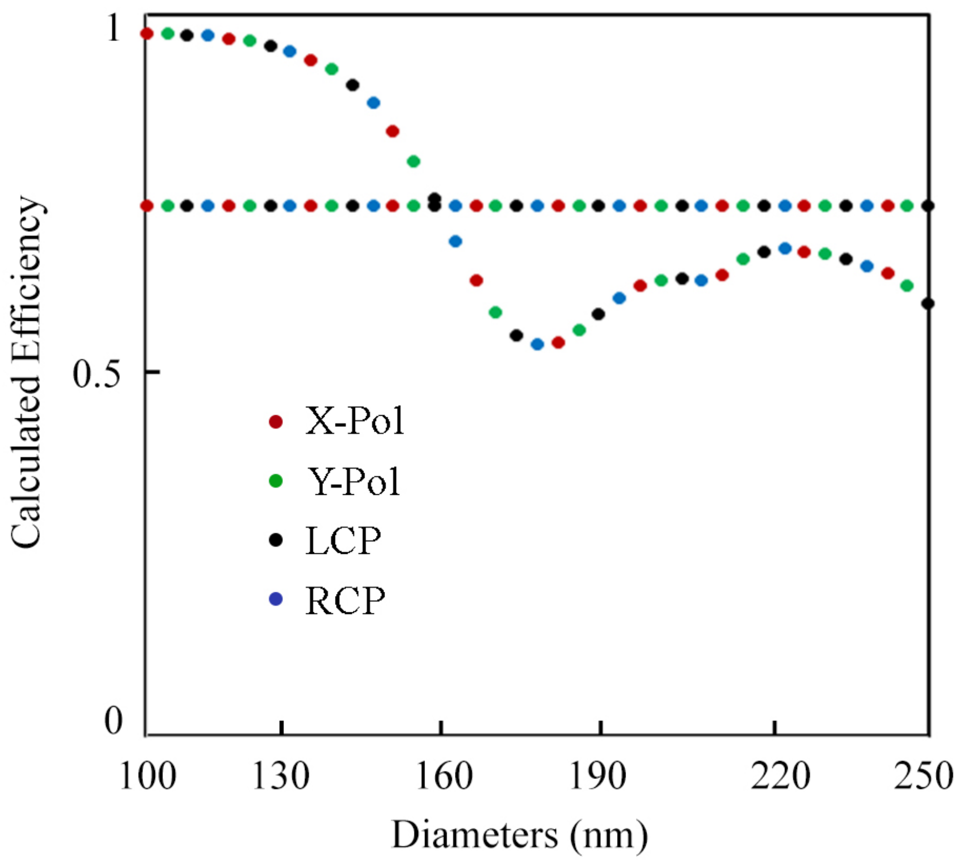


**Fig. S5.** Simulated normalised calculated efficiency of circular nanowaveguides made of a–Si:H for linear and circular polarisation. Average transmitted efficiency is observed as 73.485% proving the fundamental building block of a-Si:H as a very strong candidate for highly efficient dielectric metasurfaces in the visible spectrum. By sweeping the diameter of the nanowaveguides under different polarisation of the impinged source with fixed wavelength of 633 nm depicts strong similarity, proving the concept of polarisation insensitive of the proposed metasurface.

**Phase merging for highly focused optical vortices**

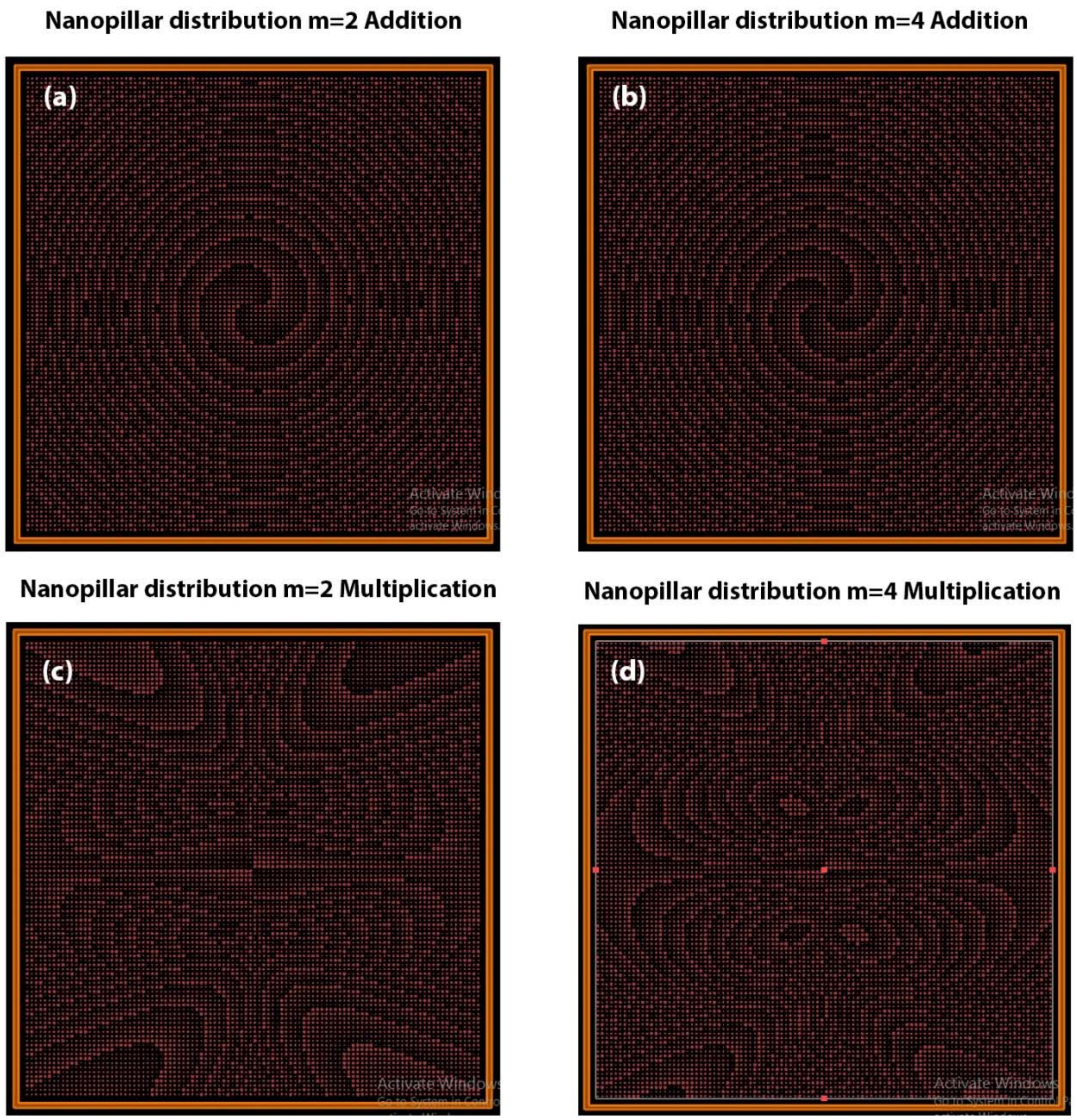


**Fig. S6.** Nanopillars distribution against phase (a, b) addition and (c, d) multiplication sign in equation 4. Phase information is designed to obtain focused optical vortex without degrading nanopillar’s helical distribution. The only option to achieve the desired focusing of the generated optical vortex is to add both profiles as their addition doesn’t affect the helical distribution of the nanopillars as given in (a) and (b). In contrast, if we multiply both phase profiles, there won’t be helical distribution of nanopillars as given in (c) and (d).

**Topological charge simulation under different polarisations**

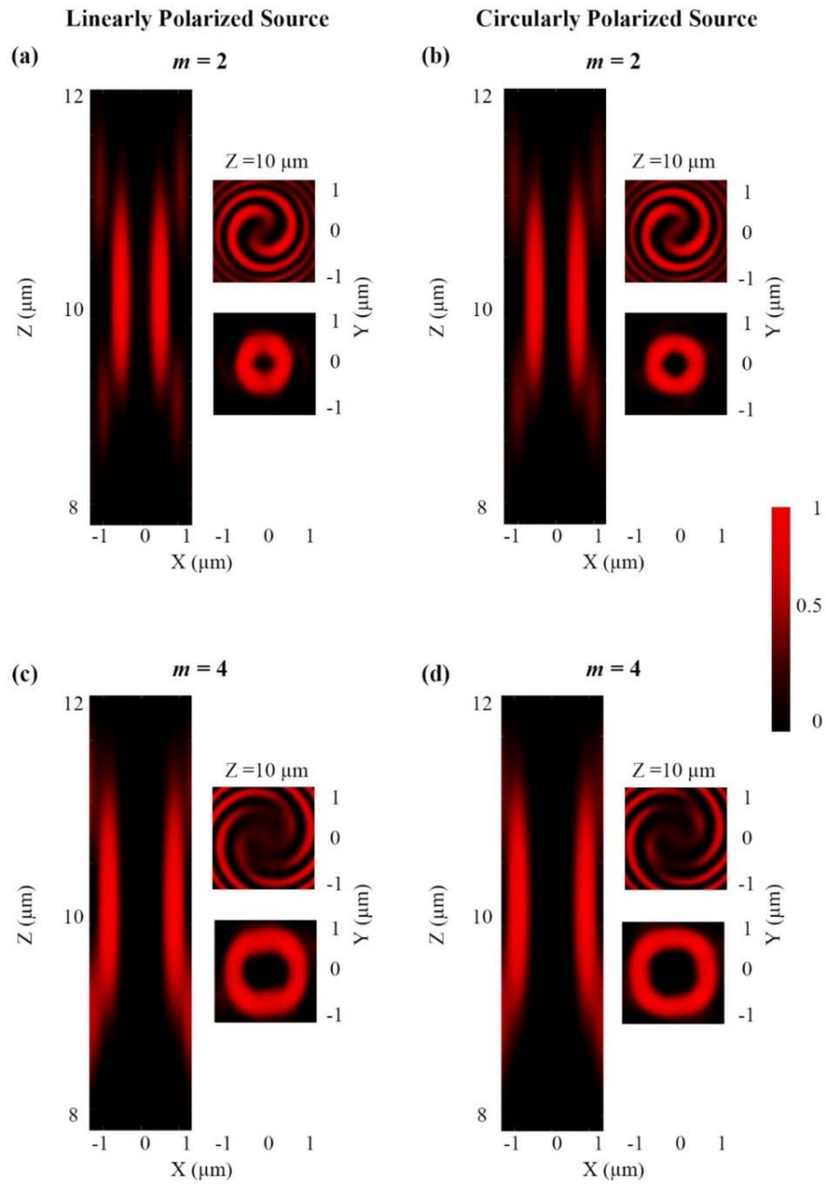


**Fig. S7.** Simulated electric field intensity distribution of optical vortex beam for topological charge $m = 2$ and 4 under different polarisation of the incident light. (a), (c) show the normalised transmitted electric field distributions, captured by the monitor placed along the *x*–*z* and *x*–*y* axis respectively, for linear polarisation of the impinged light. (b), (d) indicate the field intensity for circularly polarised plane–wave source. A clear message is revealed by the simulated response of the metasurface, that as topological charge increases from 2 to 4, the central defect or the zero–intensity region along the propagation axis and the number of spirals at the focal plane increase, validating the application of vertex beam generation via proposed.

**Magnified and tilted SEM image of the nanopillars**

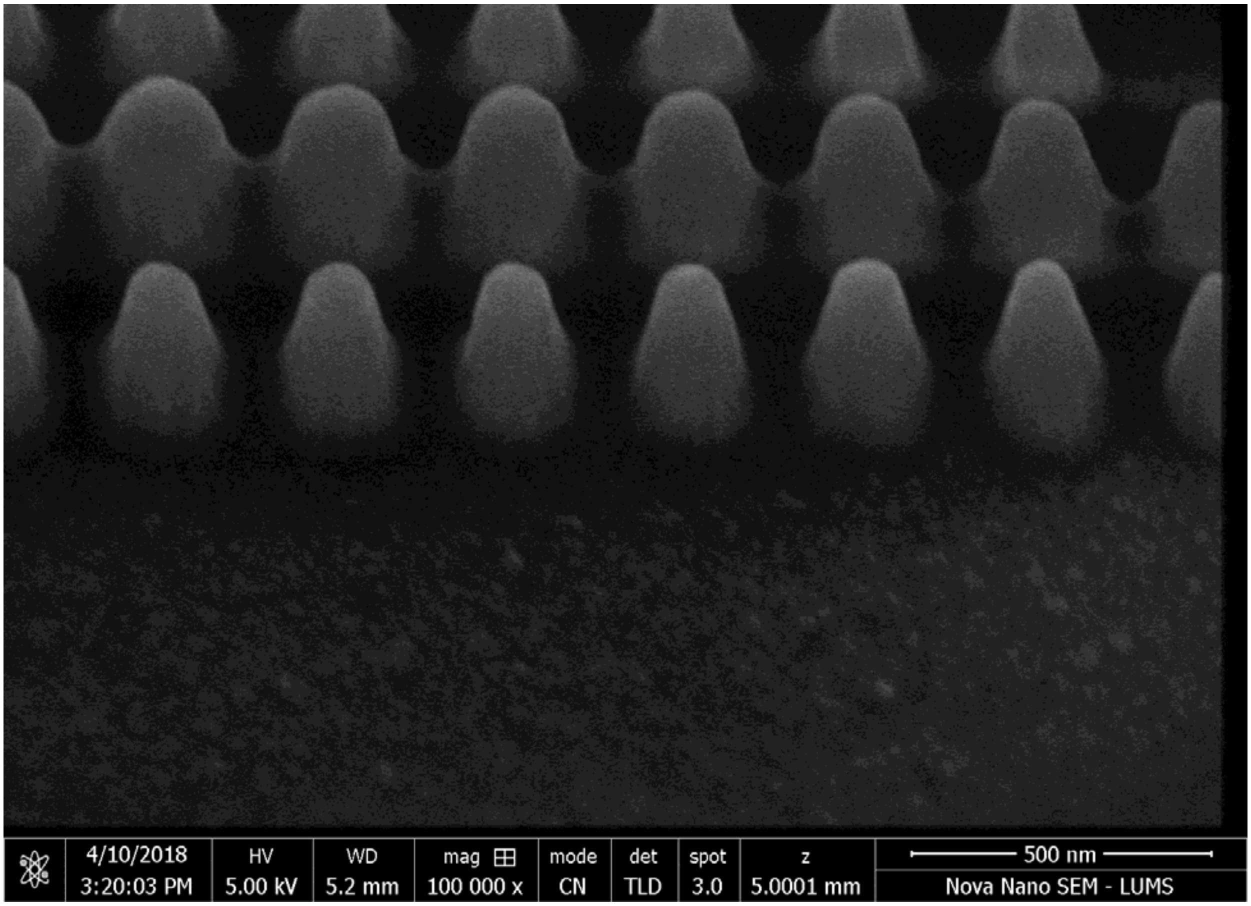


**Fig. S8.** Magnified and tilted SEM image of the fabricated nanopillars. The height of nanopillars is designed to be 400 nm and the diameter varies from 100 nm to 250 nm according to phase profiles. We measured that the height of nanopillars is around 390 nm and the diameter of pillars is around 200 nm. The etched nanopillars are slightly sloped, which is attributed to the amorphous state of the deposited silicon, and causes the phase variation and corresponding efficiency drop.

**Device operation result based on different orientation**

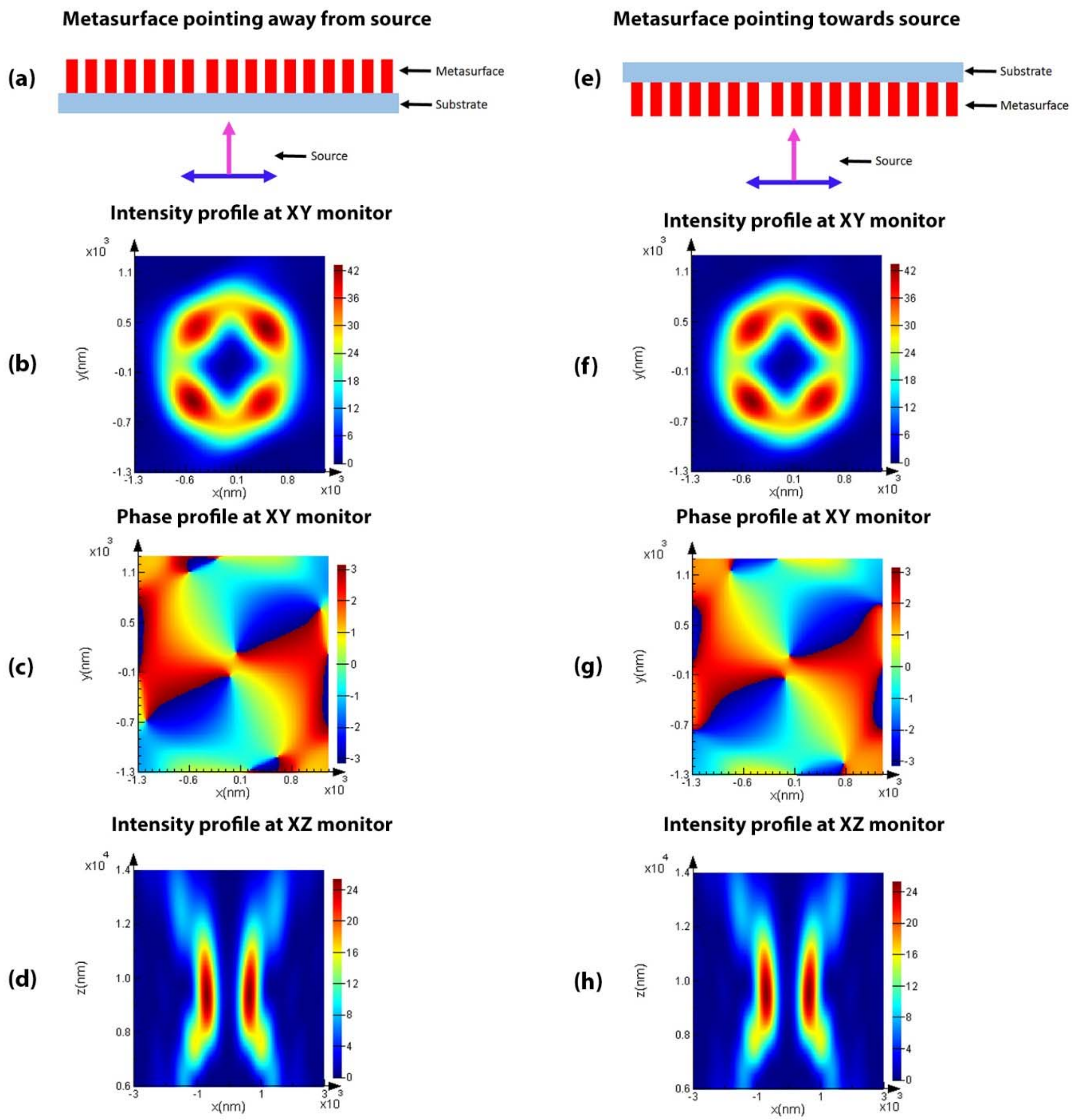


**Fig. S9.** Simulated device operation results when nanopillars point (a-d) towards or (e-h) away from the incident beam.

**Device operation results in different visible wavelength**

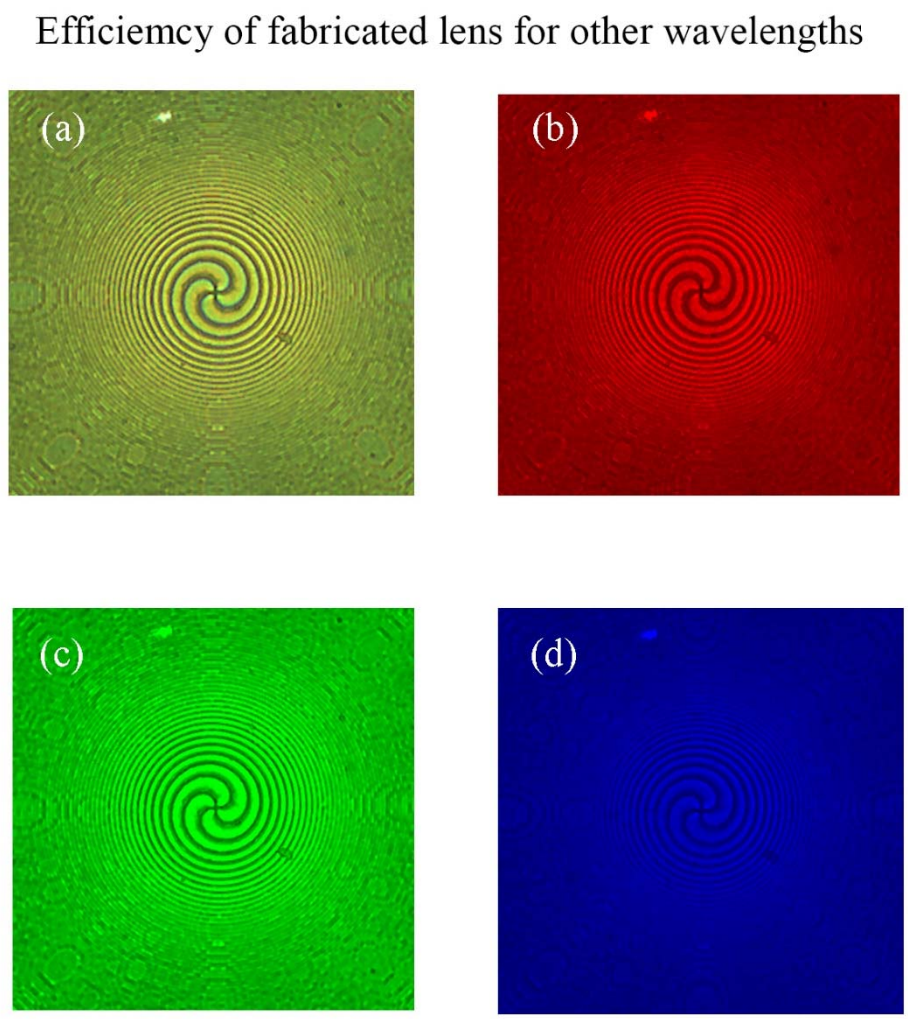


**Fig. S10.** Optical response of fabricated lens for topological charge m = 4 under (a) white, (b) red, (c) green and (d) blue incident light respectively. For wavelengths greater than 632.8 nm, the imaginary part (k) of the complex refractive index of a-Si:H exhibits smaller value results in lower absorption and higher transmission efficiency. On the other hand, for wavelengths smaller than 632.8 nm, the imaginary part (k) of a-Si:H exhibits larger value, ultimately presenting lower transmission efficiency.

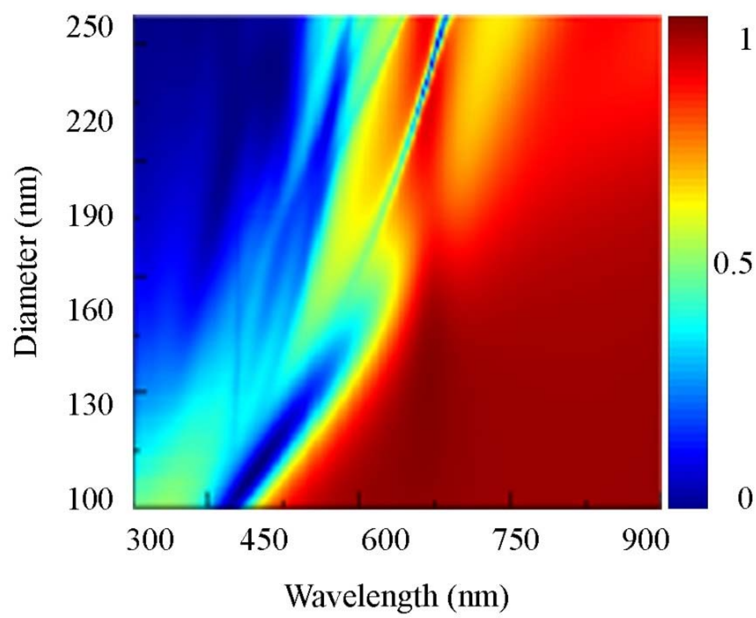


**Fig. S11.** Simulated 2D transmittance plot against wavelength and diameter of nanopillars.